International Journal of GEOMATE, March, 2026 Vol.30, Issue 139, pp.38-46
ISSN: 2186-2982 (P), 2186-2990 (O), Japan, DOI: https://doi.org/10.21660/2026.139.5245
Geotechnique, Construction Materials and Environment

EXPERIMENTAL DETERMINATION OF PENETRATION COEFFICIENTS OF VARIOUS CONCRETE TYPES UNDER HIGH-VELOCITY PENETRATING OBJECT IMPACT

Tri-Ta Nguyen[1], *Trong-Thang Dam[1], Xuan-Bang Nguyen[1], and Van-Hieu Nguyen[1]

[1]Institute of Technique for Special Engineering, Le Quy Don Technical University, Vietnam

*Corresponding Author, Received: 27 Sep. 2025, Revised: 29 Dec. 2025, Accepted: 02 Jan. 2026

ABSTRACT: Structural failures of buildings can result from high-velocity impacts on structural elements, such as collisions with vehicles, fragments from explosions, or military projectiles during warfare. These impacts may cause deep penetration and severe damage, compromising the load-bearing capacity of the structure. To estimate penetration depth, empirical formulas are commonly employed, which depend on a material-specific penetration coefficient (K_p) that must be determined experimentally. For certain concrete types, including normal concrete (B22.5) and coral concrete, this coefficient has not yet been established. This study presents experimental investigations of penetration depth in concrete specimens subjected to high-velocity impacts using bullet-shaped projectiles. Based on the test results, the penetration coefficient (K_p) was determined as $20.1 \cdot 10^{-7}$ for B22.5 concrete and $22.13 \cdot 10^{-7}$; $24.27 \cdot 10^{-7}$ (B22.5; B20) for coral concrete. This suggests that normal concrete has a higher penetration resistance than coral concrete, primarily because the coarse aggregates in normal concrete possess higher compressive strength than coral aggregates. These findings provide essential data for evaluating the impact resistance of concrete structures under high-speed object penetration, thereby contributing to the development of a database of K_p coefficients with potential applications in the practical design of structures subjected to high-velocity penetrating objects.

Keywords: High-velocity object; Penetration coefficient; Coral concrete; Compressive strength of concrete.

1. INTRODUCTION

Understanding the penetration mechanisms of high-velocity objects into solid materials is a crucial aspect in designing civil structures subjected to extreme dynamic loads. Such structures include residential buildings, protective walls, and small storage facilities, which may be impacted by high-speed collisions or debris under unexpected scenarios. Accurately predicting penetration depth, stress distribution, strain, and failure mechanisms is essential to ensure structural safety, efficient material utilization, and enhanced impact resistance.

To estimate penetration depth, numerous empirical and semi-empirical formulas have been developed and applied internationally. Some widely referenced formulas include Berezini [1] from Russia, Petry [2,3], NDRC [2–4] from the United States, ACE [3,5], and EDF [3,6,7] from France. Among these, the Berezini formula is relatively simple to apply, incorporating the penetration resistance coefficient (K_p), a quantitative parameter representing the material's resistance to penetration. The coefficient K_p reflects the combined influence of compressive strength, material density, porosity, and brittleness on penetration resistance, providing a consolidated parameter that is particularly useful for analyzing penetration mechanisms and numerical simulations. Employing the Berezini formula allows direct evaluation of K_p, enabling standardized comparison between materials, especially those with complex microstructures like coral aggregate concrete, where penetration and stress distribution differ from ordinary concrete.

In this study, two types of concrete are investigated: ordinary concrete of grade B22.5 and coral aggregate concrete of grade B20; B22.5 concrete is commonly used in civil structures due to its balanced mechanical properties, sufficient compressive strength, and cost-effectiveness. In contrast, coral aggregate concrete is frequently applied in coastal and island regions, utilizing locally available coral as aggregate, which reduces transportation and material extraction costs. This type of concrete exhibits high porosity, low density, and brittle behavior, leading to complex penetration and failure mechanisms when subjected to high-velocity impacts. These characteristics render mechanical parameters such as compressive strength, density, stress wave propagation, and crack development critical for predicting K_p and overall structural response.

To investigate penetration mechanisms and determine K_p, this study integrates field impact experiments and finite element simulations using Abaqus/Explicit. Both types of concrete are modeled using the Holmquist–Johnson–Cook (HJC) model, which captures nonlinear behavior, strain-rate dependence, progressive failure, and stress wave propagation in brittle materials like coral aggregate concrete. Field experiments measure key parameters including penetration depth, residual velocity,

deformation, and material damage patterns, while numerical simulations provide detailed insight into stress distribution, plastic strain, crack propagation, and local failure progression. Comparison of experimental and numerical results allows assessment of model accuracy and reliability, identification of main factors influencing K_p such as compressive strength, density, porosity, and aggregate structure, and the formulation of calibrated relationships consistent with the actual mechanical behavior of each concrete type.

The results contribute to expanding the dynamic material property database, supporting the design of civil structures under impact loads and providing a comprehensive methodology combining experimental and numerical approaches. Accurate determination of K_p not only improves the prediction of structural response but also facilitates optimized material use, reduced construction costs, and enhanced structural safety. Moreover, this research framework can be extended to study other specialized construction materials lacking empirical data, serving as a basis for developing numerical models to predict failure in brittle, porous, or non-traditional materials.

The integrated approach combining theoretical analysis, field experimentation, and numerical simulation establishes a rigorous scientific methodology applicable to other construction material studies, helping civil engineers make informed and optimized design decisions under extreme dynamic loading. Additionally, establishing a comprehensive and reliable K_p database plays a crucial role in developing standardized guidelines for high-velocity impact-resistant materials for civil infrastructure in the future.

2. RESEARCH SIGNIFICANCE

This research is novel in that it experimentally determines the penetration coefficient (Kp) for B22.5 normal concrete and coral concrete, materials for which reliable high-velocity impact data have been unavailable. Unlike previous studies that rely mainly on foreign material databases, this work provides original, material-specific Kp values derived from controlled penetration tests using bullet-shaped projectiles. The study clarifies the distinct penetration resistance and failure mechanisms of coral and normal concrete, highlighting the role of aggregate strength. These original findings significantly improve penetration prediction accuracy and establish new reference data for impact-resistant structural design in both civil and military engineering.

3. THEORETICAL BASIS FOR DETERMINING PENETRATION COEFFICIENT OF HIGH-VELOCITY PENETRATING OBJECTS

3.1 Theoretical Background

The penetration process of a high-velocity object into a structure is fundamentally a mechanics problem involving a high-strength object impacting a material with lower strength—such as coral concrete, soil, or regular concrete—resulting in penetration.

Penetration depth depends on various factors: the object's kinetic energy, the target material's resistance (represented by the K_p coefficient), the impact duration, impact angle, shape, and diameter of the penetrating object (Fig.1).

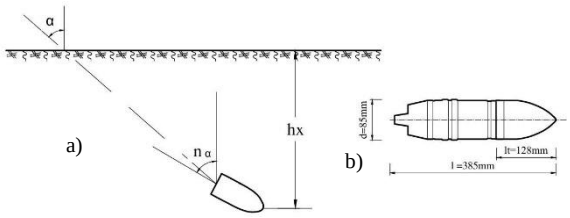

Fig. 1. Determination of the penetration depth of a bullet-shaped object: a. Penetration depth of the object; b. Length of the tapered (nose) section of the object.

Based on theoretical analysis and experimental data, the penetration depth (h_p) of a high-velocity penetrating object can be determined using the Berezini formula (Russian standard), which combines theoretical and empirical approaches. This formula includes variables such as [1, 8-10]:

$$h_p = \lambda_1.\lambda_2.K_p.\frac{P}{d^2}.V_0.\cos\left(\frac{1+n}{2}\right)\alpha \quad (1)$$

Where:

h_p - the penetration depth of the high-velocity penetrating object, in meters (m).

λ_1 - coefficient that depends on the tapered (nose) shape of the object (see Fig.1b), and is calculated using the following formula:

$$\lambda_1 = \sqrt{\frac{l_t}{1,5d}} \quad (2)$$

λ_2: the shape coefficient, calculated as follows:

$$\lambda_2 = 2,8\sqrt[3]{d} - 1,3\sqrt{d} \quad (3)$$

l_t: the length of the tapered nose section of the penetrating object (m);

P: weight of the penetrating object (kg);

d: diameter of the penetrating object's body (m);

V_0: initial impact velocity (m/s);

α: impact angle, in degrees;

n: deflection coefficient of the projectile in the target medium, determined based on experimental results as follows:

+ For concrete and reinforced concrete structures:

if $\frac{l_t}{d} \geq 2$ then n = 1,5;

if $\frac{l_t}{d} < 2$ then n = 2.

+ For soft soil environments, n=1;

- The penetration coefficient K_p is determined experimentally.

Russian engineers have experimentally established the values of K_p for various target materials, as shown in Table 1 below.

Table 1. Penetration coefficients K_p for different materials [1, 9]

No.	Material Description	K_p
1	Newly filled loose soil	130.10^{-7}
2	Dense sand with natural moisture	45.10^{-7}
3	Water-saturated sand	68.10^{-7}
4	Silty sand	50.10^{-7}
5	Clayey soil	60.10^{-7}
6	Medium compact clay	70.10^{-7}
7	Non-fractured limestone or sandstone	20.10^{-7}
8	Granite or gneiss	16.10^{-7}
9	Pine wood	50.10^{-7}
10	Rubble stone masonry with cement mortar	20.10^{-7}
11	Dry-laid rubble stone masonry	30.10^{-7}
12	Brick masonry with cement mortar	25.10^{-7}
13	Dry-laid brickwork	30.10^{-7}
14	Rubble concrete	16.10^{-7}
15	Granite rubble concrete (grade 250)	12.10^{-7}
16	Granite rubble concrete (grade 400)	10.10^{-7}
17	Reinforced concrete with limestone aggregate (grade 250)	11.10^{-7}
18	Reinforced concrete with limestone aggregate (grade 400)	8.10^{-7}
19	Reinforced concrete with limestone aggregate	10.10^{-7}
20	Reinforced concrete (grade 500–600)	7.10^{-7}

Analysis of Equation (1) shows that the penetration coefficient K_p does not depend on the type of penetrating object or its flight characteristics. Instead, it is considered a material-specific constant that characterizes the material's resistance to penetration. The coefficient K_p is determined primarily by the mechanical properties of the target material.

$$K_p = \frac{h_p.d^2}{\lambda_1.\lambda_2.P.V_0} . \quad (4)$$

3.2. Numerical Simulation for Preliminary Determination of Specimen Dimensions Under High-Velocity Impact

To perform high-velocity impact experiments, it is necessary to design appropriate test specimens that can withstand the impact without being fully penetrated. The penetrating object must be stopped within the specimen to allow for accurate measurement of penetration depth, which in turn helps determine proper specimen dimensions for repeated testing.

ABAQUS software was selected for numerical simulation due to its powerful capabilities in modeling structures under complex dynamic conditions. It integrates multiple methods [11-17]:

- Finite Element Method (FEM) for small deformation regions far from the impact zone;

- Discrete Element Method (DEM) for fracture zones;

- Smoothed Particle Hydrodynamics (SPH) for the impact center and explosion zones.

The scope of problem-solving using ABAQUS ranges from relatively simple linear analyses—such as blast or impact problems—to complex nonlinear simulations. ABAQUS provides a comprehensive element library, allowing the modeling of virtually any geometric shape. Its material library supports the simulation of a wide variety of structural materials, including metals, rubber, polymers, composites, and reinforced concrete.

Given the capabilities of the Abaqus software, it was selected to perform numerical simulations to preliminarily determine the dimensions of the high-velocity impact test specimens, thereby reducing the cost of full-scale field experiments.

3.2.1. Penetrating Object Parameters

The high-velocity penetrating object was modeled as a steel body with the following parameters [18]:

Table 2. Penetration object Parameters

Parameter	Unit	Value
Mass (P)	kg	9,58
Diameter (d)	m	0,085
Total length (l)	m	0,385
Tapered nose length (l_t)	m	0,128
Impact velocity (V_0)	m/s	580
Impact angle (α)	(^{0})	0

The steel material was modeled using the Johnson–Cook constitutive model with parameters shown below [19]:

Table 3. Johnson–Cook Parameters for Steel

No.	Parameter	Unit	Value
1	Young's modulus	(N/m^2)	2.10^{11}
2	Poisson's ratio		0,3
3	A		$2.64.10^8$
4	B		$1,3.10^8$
5	n		0.0915
6	T_{melt}	(^{0}K)	1800
7	T_{room}	(^{0}K)	293.2
8	m		1
9	Density	(kg/m^3)	7850
10	d1		0.05
11	d2		3.44
12	d3		2.12
13	d4		0.002
14	d5		0.61
15	C		0.017
16	strain rate		1.0

3.2.2. Material model for B22.5-Grade concrete and B20-grade coral concrete

The concrete was modeled using the Holmquist–Johnson–Cook (HJC) model, with parameters as follows in Tab. 4 [20, 21]:

Table 4. HJC Model Parameters for normal concrete and coral concrete.

No.	Parameter	Unit	normal concrete	coral concrete
1	Density (ρ_0)	kg/m³	2440	2106
2	G	Pa	$11.608\cdot10^9$	$10.677\cdot10^9$
3	A		0.79	0.79
4	B		1.405	1.405
5	C		0.007	0.007
6	N		1.085	1.085
7	e_{fmin}		0.0016	0.0016
8	T_c	Pa	$3.387\cdot10^6$	$3.193\cdot10^6$
9	f_c	Pa	$28.9\cdot10^6$	$25.69\cdot10^6$
10	S_{max}		7	7
11	P_{crush}	Pa	$9.633\cdot10^6$	$8.563\cdot10^6$
12	μ_{crush}		0.0007	0.0007
13	P_{lock}	Pa	$1\cdot10^9$	$1\cdot10^9$
14	μ_{lock}		0.08	0.08
15	μ		0.2	0.2
16	D_1		0.04	0.04
17	D_2		1.0	1.0
18	K_1	Pa	$85\cdot10^9$	$85\cdot10^9$
19	K_2	Pa	$-117\cdot10^9$	$-117\cdot10^9$
20	K_3	Pa	$208\cdot10^9$	$208\cdot10^9$
21	E	Pa	$27.861\cdot10^9$	$25.625\cdot10^9$

3.2.3. Air model

Assuming an initial state of equilibrium, the ideal gas equation of state is defined as in Equation (5) [22, 23]:

$$p = (\gamma - 1)\rho e \,. \quad (5)$$

Where: p is the hydrostatic pressure, ρ is the density of air, e is the specific internal energy, $\gamma = 1 + \frac{R}{c_v}$, is the adiabatic index (heat capacity ratio). The parameters used for modeling air are listed in Table 5.

Table 5. Parameters for Air Model [24, 25]

Parameter	Unit	Value
ρ (density of air)	kg/m³	1,2
p	MPa	0,0085
e (specific internal energy)	J/kG	193300
γ (adiabatic index)	m	1,4
c_v	J/kG.K	716,4
T_0	(^{0}K)	288

The computational model for determining the penetration depth of a bullet-shaped penetrating object into normal concrete and coral concrete is illustrated in Fig. 2.

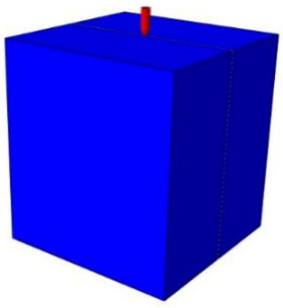

Fig. 2. Computational model for penetration depth into the test specimen.

3.2.4. Simulation results

Simulation results of the high-velocity penetrating object impacting normal concrete are shown in Fig. 3 below:

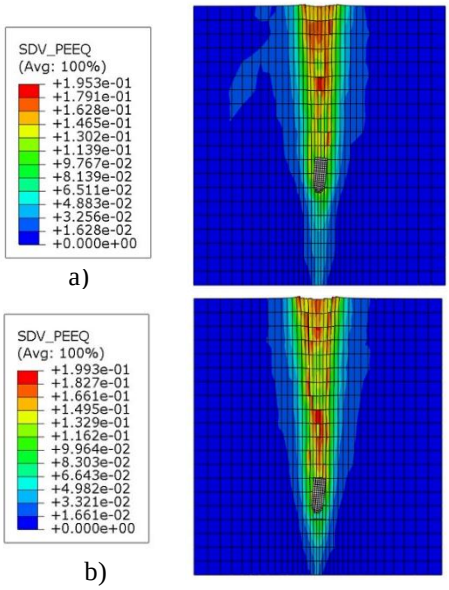

Fig. 3. Simulation results of penetration in B22.5-grade concrete (a) and B20-grade coral concrete (b).

The graph showing the relationship between impact velocity and penetration depth over time is presented in Fig. 4.

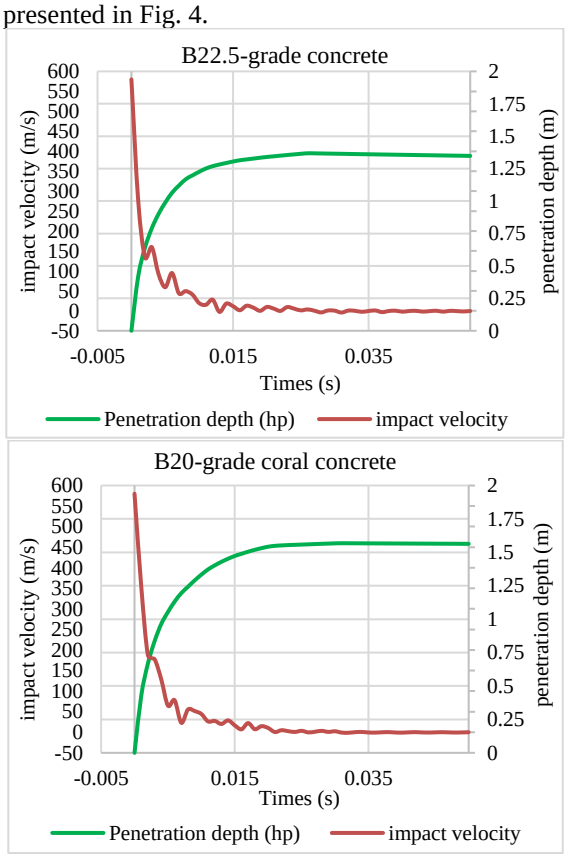

Fig. 4. Penetration depth and impact velocity versus time.

Observation: Based on the simulation results of a bullet-shaped high-velocity penetrating object impacting the concrete specimens (Fig.s 3 and 4), it was found that at an impact velocity of 580 m/s, the penetration depth was 1.35 m for normal concrete and 1.57 m for coral concrete. The greater penetration depth in coral concrete is primarily attributed to its lower compressive strength and higher porosity compared to normal concrete, which reduces its resistance to high-velocity impacts.

4. EXPERIMENTAL DETERMINATION OF PENETRATION DEPTH IN NORMAL AND CORAL CONCRETE

4.1. Objective

The experiment aimed to determine the penetration depth of high-velocity penetrating objects with a diameter of 85 mm and bullet-like geometry (fig. 1.b), by impacting normal concrete and coral concrete specimens. The penetration depth data would be used to calculate the penetration coefficient (K_p) for each concrete type.

4.2. Requirements

Concrete specimens must be prepared in accordance with predefined mix designs. Each test sample must be accompanied by documentation (mixing log, strength test data, and sample ID).

Testing devices (launching equipment, projectiles, high-speed cameras) must be fully safe and operated by specialized personnel.

During each test, all relevant data must be recorded in detail to support post-experiment analysis.

4.3. Experimental Method

High-velocity launching equipment was used to project penetrating objects directly into the prepared concrete specimens. The materials tested included:

- B22.5-grade normal concrete
- B20-grade coral concrete, both cured for 28 days.

The mix proportions of B22.5 concrete and B20- and B22.5-grade coral concrete were designed, and the corresponding laboratory-measured compressive strengths are summarized below:

Table 6. Mix proportions of selected concrete types

Concrete type	Water-cement ratio	Cement (kg)	Sand (kg)	Coarse aggregate (kg)	Water (litre)	Compressive strength (MPa)		
						R7	R14	R28
B20*	0.60	390	780	950	234	19.36	23.99	26.35
B22.5*	0.58	440	860	900	255	24.98	27.04	30.12
B22.5	0.5	390	620	1164	195	28.12	31.68	35.25

** Note: Coral concrete utilizes coral sand, coral aggregate, and seawater as constituent materials.*

Due to the difficulty in achieving laboratory-level strength control for coral concrete specimens fabricated under field conditions, a B22.5 mix design was employed to ensure a compressive strength greater than 25 MPa during the experiments.

Penetration depth was measured using one of the following methods:

- Direct measurement with a standard depth gauge;
- Ultrasonic testing (if necessary);
- Cutting the specimen to directly observe the projectile's final position.

All safety measures were strictly implemented in compliance with the applicable regulations [26], and the experimental protocols and test plans were formally reviewed and approved by the relevant authorities.

4.4. Experimental Equipment

4.4.1. Concrete specimen mounting stand

The concrete test specimens were placed on a target platform made of concrete, located 700 meters from the launching position (Fig. 5).

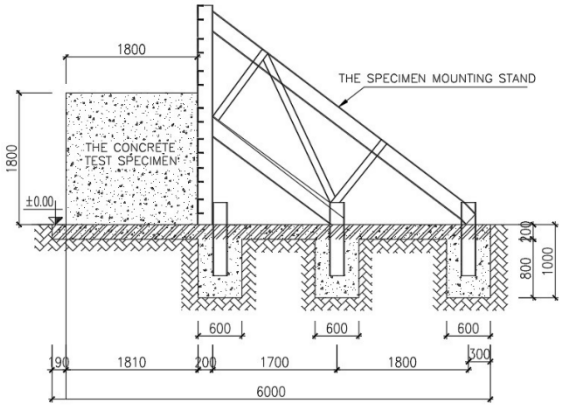

Fig. 5. Support platform and concrete specimen mounting stand used in the experiment

4.4.2. Equipment for measuring impact velocity

To measure the impact velocity at the concrete surface, modern equipment was used, including high-speed cameras (fig.6), radar sensors, and still-image capture systems.

Fig. 6. High-speed camera system for measuring

The penetration depth was determined by measuring, with a steel ruler, the distance from the concrete surface to the tip of the penetrating object embedded within the 85 mm diameter hole in the concrete specimens.

4.5. Test Specimens

Based on the simulation results described in Section 2.2, the predicted penetration depth of a bullet-shaped object is approximately 1.35 meters for normal concrete and 1.57 meters for coral concrete.

To ensure safety during the experiments, the specimen dimensions were set to 1.8 × 1.8 × 1.8 meters (Fig. 5). Two concrete types were prepared – normal concrete and coral concrete - with 10 specimens of each type. Due to launch accuracy constraints, only eight specimens yielded valid results.

The results of the penetration depth measurements and the compressive strength tests conducted (R14 and R28) are presented in Table 8.

5. RESULTS AND DISCUSSION

5.1. Experimental Results

The experimental results for determining the penetration depth of high-velocity penetrating objects into normal concrete (Fig. 7) and coral concrete specimens (Fig. 8) are summarized in the Table 7. As shown in Table 7, the depth of penetration varies depending on the impact velocity.

Table 7. Measured penetration depth and impact velocity results

Concrete type	Specimen ID	R14 (MPa)	R28 (MPa)	Penetration depth (cm)	Impact velocity (m/s)
Grade concrete	BT1	35.11	38.15	109.0	567.5
	BT2	18.82	30.37	135.9	578.2
	BT3	22.44	30.96	125.7	590.2
	BT4	23.41	30.67	123.0	560.3
	BT5	23.41	30.67	130.2	562.0
	BT6	25.52	34.01	117.7	585.2
	BT7	28.56	36.61	113.0	574.8
	BT8	29.24	37.42	110.7	569.8
Coral concrete	BTSH1	26.00	27.33	154.0	578.2
	BTSH2	28.52	31.11	139.5	567.5
	BTSH3	28.30	32.44	134.0	565.8
	BTSH4	26.00	27.33	150.0	573.4
	BTSH5	28.52	31.11	142.8	564.2
	BTSH6	25.67	28.52	146.6	566.8
	BTSH7	25.71	29.22	142.3	575.4
	BTSH8	26.91	30.58	136.9	568.2

Photographs of the B22.5 concrete and coral concrete test specimens after testing are presented in the following figures:

Fig. 7. High-velocity impact test results on normal concrete

Fig. 8. High-velocity impact test results on coral concrete

5.2. Processing of Experimental Results

Based on the experimental results for each target's strength grade, including the measured penetration depth and impact velocity, Equation (4) was used to calculate the penetration coefficient K_p for each specimen. As the targets had different strength grades but similar impact velocities, the calculated K_p values were used to establish a regression function in Microsoft Excel, describing the relationship between concrete strength grade and penetration coefficient. From this function, the K_p values for normal concrete and coral concrete were obtained.

5.2.1. Calculation of the penetration coefficient for B22.5-grade concrete

The calculated K_p values for normal concrete are shown in the following table.

Table 8. Calculated penetration coefficients of high-velocity penetrating objects in normal concrete specimens

Specimen ID	Compressive strength (Mpa)	Penetration depth (cm)	Impact velocity (m/s)	λ_1	λ_2	Experimental penetration coefficient K_p
BT1	38.15	109.0	567.5	1.0	0.852	$17.00 \cdot 10^{-7}$
BT2	30.37	135.9	578.2	1.0	0.852	$20.80 \cdot 10^{-7}$
BT3	30.96	125.7	590.2	1.0	0.852	$18.90 \cdot 10^{-7}$
BT4	30.67	123.0	560.3	1.0	0.852	$19.43 \cdot 10^{-7}$
BT5	30.67	130.0	562.0	1.0	0.852	$20.48 \cdot 10^{-7}$
BT6	34.01	117.7	585.2	1.0	0.852	$17.80 \cdot 10^{-7}$
BT7	36.61	113.0	574.8	1.0	0.852	$17.40 \cdot 10^{-7}$
BT8	37.42	110.7	569.8	1.0	0.852	$17.20 \cdot 10^{-7}$
average	33.61	120.62	573.5	1.0	0.852	$18.62 \cdot 10^{-7}$

Based on the experimental results of high-velocity impact on normal concrete shown in Table 8, a regression analysis using Microsoft Excel was performed. The resulting relationship between concrete strength grade and the penetration coefficient K_p is illustrated in Fig. 9.

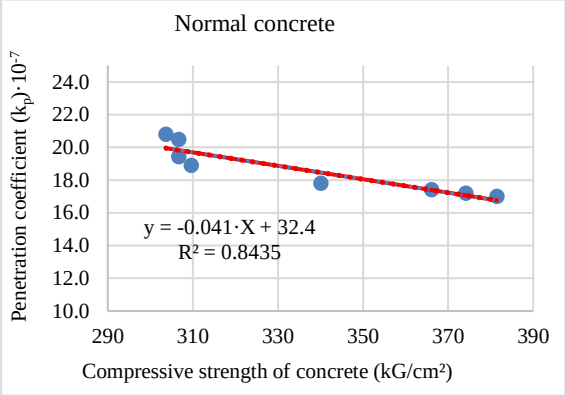

Fig. 9. Relationship between penetration coefficient and compressive strength of concrete

5.2.2. Calculation of the penetration coefficient for B20-Grade coral concrete

The calculated K_p values for coral concrete are shown in the following table.

Table 9. Calculated penetration coefficients of high-velocity penetrating objects in coral concrete specimens

Specimen ID	Compressive strength (Mpa)	Penetration depth (cm)	Impact velocity (m/s)	λ_1	λ_2	Experimental penetration coefficient K_p
BTSH1	27.33	154.0	578.2	1.0	0.852	$23.58 \cdot 10^{-7}$
BTSH2	31.11	139.5	567.5	1.0	0.852	$21.76 \cdot 10^{-7}$
BTSH3	32.44	134.0	565.8	1.0	0.852	$20.96 \cdot 10^{-7}$
BTSH4	27.33	150.0	573.4	1.0	0.852	$23.16 \cdot 10^{-7}$
BTSH5	31.11	142.8	564.2	1.0	0.852	$22.40 \cdot 10^{-7}$
BTSH6	28.52	146.6	566.8	1.0	0.852	$22.90 \cdot 10^{-7}$
BTSH7	29.22	142.3	575.4	1.0	0.852	$21.89 \cdot 10^{-7}$
BTSH8	30.58	136.9	568.2	1.0	0.852	$21.32 \cdot 10^{-7}$
average	29.71	143.26	569.9			$21.78 \cdot 10^{-7}$

Based on the experimental results of high-velocity impact on coral concrete presented in Table 9, a regression analysis was performed using Microsoft Excel. The resulting relationship between the concrete strength grade and the penetration coefficient K_p is shown in Fig. 10.

The results of the field experiment on high-velocity impact of a bullet-shaped projectile on normal concrete target yielded a regression equation of the form:

$$K_{p1} = (-0.041 \cdot X + 32.4) \cdot 10^{-7} . \quad (6)$$

Using Equation (6), the penetration coefficient for B22.5 normal concrete (X = 300) is calculated as:

$$K_{p1} = (-0.041 \cdot 300 + 32.4) \cdot 10^{-7} = 20{,}1 \cdot 10^{-7} .$$

Similarly, the results of the high-velocity impact test on a coral concrete target yielded a regression equation of the form:

$$K_{p2} = (-0{,}0427 \cdot X + 34.94) \cdot 10^{-7} . \quad (7)$$

Using Equation (7), the penetration coefficients for coral concrete B20, B22.5 are calculated as:

$$K_{p2}^{B20} = (-0.0427 \cdot 250 + 34.94) \cdot 10^{-7} = 24.27 \cdot 10^{-7}$$

$$K_{p2}^{B22.5} = (-0.0427 \cdot 300 + 34.94) \cdot 10^{-7} = 22.13 \cdot 10^{-7}$$

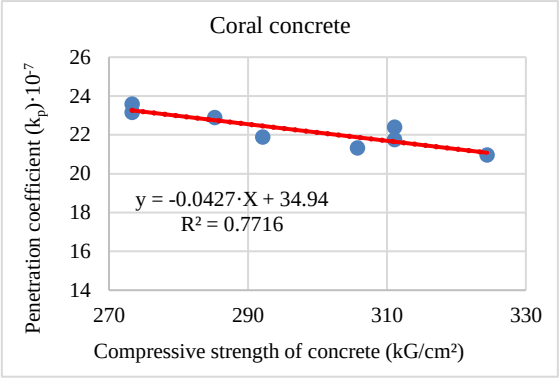

Fig. 10. Penetration coefficient and compressive strength of coral concrete.

6. CONCLUSION

The experimental determination of the penetration coefficient for B22.5 concrete using high-velocity impact tests with bullet-shaped projectiles yielded results that closely align with those of rubble concrete listed in Table 1. This indicates the reliability of the experimental method and results.

The experimental determination of the penetration coefficient for coral concrete B20, B22.5 and normal concrete B22.5 under similar high-velocity impact conditions will serve as a reference for supplementing and refining the classification of new materials in Table 1.

The results also indicate that normal concrete B22.5 exhibits a lower penetration coefficient (Kp = $20.1 \cdot 10^{-7}$) compared with coral concrete of grades B22.5 and B20, which show Kp values of $22.13 \cdot 10^{-7}$ and $24.27 \cdot 10^{-7}$, respectively. This suggests that normal concrete has a higher penetration resistance than coral concrete, primarily because the coarse aggregates in normal concrete possess higher compressive strength than coral aggregates.

Further experimental studies involving high-velocity impact on a larger number of specimens and wider range of materials, including reinforced concrete, are necessary to develop a comprehensive database of penetration coefficients. Such data will support more realistic and accurate calculations in the design of protective structures.

7. ACKNOWLEDGEMENT

The authors gratefully acknowledge the support of Le Quy Don Technical University during the experimental process.

8. REFERENCES

1. Lisogor A.A., Защитные конструкции оборонительных сооружений и их расчет. Московский геолого-разведочный институт им. С. Орджоникидзе, Спецкафедра, Moscow, 1958, pp.1–500.
2. Li Q.M., Reid S.R., Wen H.M., Telford A.R., Local impact effects of hard missiles on concrete targets. International Journal of Impact Engineering, 32(1–4), 2005, pp.224–284. https://doi.org/10.1016/j.ijimpeng.2005.04.007
3. Abdul Rahman I., Ahmad Zaidi A.M., Latif Q.B.I., Review on Empirical Studies of Local Impact Effects of Hard Missile on Concrete Structures. International Journal of Sustainable Construction Engineering and Technology, 1(1), 2011, pp.73–98. https://publisher.uthm.edu.my/ojs/index.php/IJSCET/article/view/53
4. NDRC, Effects of Impact and Explosion. Summary Technical Report of Division 2, Vol. 1, Washington, DC: National Defense Research Committee, 1946, pp.1–120.
5. ACE, Fundamentals of Protective Design. Report AT120 AT1207821, Washington, DC: Army Corps of Engineers, Office of the Chief of Engineers, 1946, pp.1–80.
6. Rahman I.A., Ibrahim A., Jamaluddin N., Noor N.M., A review on empirical studies of local impact effects of concrete structures against ballistic force under missile impact. International Journal of Sustainable Construction Engineering & Technology, 1(1), 2010, pp.89–102. https://publisher.uthm.edu.my/ojs/index.php/IJSCET/article/download/53/12
7. U.S. Nuclear Regulatory Commission, Methodology for Performing Aircraft Impact Assessments. Washington, DC: NRC, 2011, Report No.: NUREG/CR-7007, pp.1–150. https://www.nrc.gov/docs/ML1114/ML111440006.pdf
8. Thuy N.N., Loi V.D., Hoang T.M., Experimental study on determining the penetration depth of projectiles into concrete. Journal of Building Materials Research and Development, 11(3), 2021, pp.62–66. https://doi.org/10.54772/jomc.3.2021.74
9. Hieu N.V., Khanh D.D., Bang N.X., Assessment of penetration resistance of sand materials for aircraft protection fortifications. Vietnam Journal of Science and Technology, Version B, 2025, pp.1–12. https://doi.org/10.31276/VJST.2025.3261
10. Ta N.T., Tuan H.Q., Calculate the penetration depth of bomb into different structures by particle flow code. Journal of Construction, 7, 2017, pp.152–154.
11. Dassault Systèmes Simulia Corp., ABAQUS Theory Manual, Providence, RI, 2011, pp.1–600. https://www.3ds.com/products-services/simulia/products/abaqus
12. Dassault Systèmes Simulia Corp., Abaqus Analysis User's Manual, Version 6.6, Washington University in St. Louis, 2011, pp.1–500. https://classes.engineering.wustl.edu/2009/spring/mase5513/abaqus/docs/v6.6/books/usb/default.htm
13. Akhmad R.H.P., Tavio, Influence of seawater on strength of concrete beams strengthened with glass fiber reinforced polymer sheet. International Journal of GEOMATE, 26(117), 2024, pp.35–42. https://geomatejournal.com/geomate/article/view/4330/3400
14. Setyowulan D., Yamao T., Hamamoto T., Suryo E.A., Arifi E., Nuralinah D., Comparison study on the dynamic response of reinforced concrete abutments. International Journal of GEOMATE, 21(83), 2021, pp.101–108. https://geomatejournal.com/geomate/article/view/718/593
15. Tran T.H., Vu Q.A., Mai V.C., Comprehensive evaluation of flexural capacity calculation methods for ultra high performance concrete girders: Experiments, simulations, and standards. International Journal of GEOMATE, 28(129), 2025, pp.76–83. https://geomatejournal.com/geomate/article/view/4891/3637
16. Effect of crest shape on the structural behavior of double curvature concrete arch dam. International Journal of GEOMATE, 1(1), 2011, pp.59–65. https://geomatejournal.com/geomate/article/view/111/2644
17. Khassaf S.I., Al-Taie E.A., Ali N.S., Mahdi A.J., Effect of contraction joints on the structural performance of arch dam. International Journal of GEOMATE, 19(71), 2020, pp.219–227. https://geomatejournal.com/geomate/article/view/1076/924
18. Bang N.X., Ta N.T., Using the simplified concrete damage plasticity model in studying the penetration depth in concrete. Defect and Diffusion Forum, 2024, pp.1–12. https://doi.org/10.4028/p-81pkw0
19. Johnson G.R., Cook W.H., Fracture characteristics of three metals subjected to various strains, strain rates, temperatures and pressures. Engineering Fracture Mechanics, 21(1), 1985, pp.31–48. https://doi.org/10.1016/0013-7944(85)90052-9
20. Holmquist T.J., Johnson G.R., Cook W.H., A computational constitutive model for concrete

subjected to large strains, high strain rates and high pressures. In: Warhead mechanisms, terminal ballistics, 2, 1993, pp.591–600.
21. Johnson G.R., Beissel S.R., Holmquist T.J., Frew D.J., Computed radial stresses in a concrete target penetrated by a steel projectile. In: Proceedings of the 5th International Conference on Structures Under Shock and Impact, Greece, 1998, pp.793–806.
22. Fryxell B., Olson K., Ricker P., Timmes F.X., Zingale M., Lamb D.Q., et al., FLASH: An adaptive mesh hydrodynamics code for modeling astrophysical thermonuclear flashes. The Astrophysical Journal Supplement Series, 131(1), 2000, pp.273–334. https://doi.org/10.1086/317361
23. Dullemond C.P., Numerical fluid dynamics lecture notes: Chapter 1 – Equations of hydrodynamics. Heidelberg: University of Heidelberg, 2011, pp.1–60. https://www.ita.uni-heidelberg.de/~dullemond/lectures/num_fluid_2011/Chapter_1.pdf
24. Bang N.X., Chinh M.V., Study on shock wave pressure under simultaneous explosion. Journal of Science and Technology in Construction, Hanoi University of Civil Engineering, 17(4V), 2023, pp.168–178. https://doi.org/10.31814/stce.huce2023-17(4V)-14
25. Khan A., Noreen A., Ali I., Shahzada K., Azmatullah D., Approximation of Confined Dry-Stacked Interlocking Masonry Wall against Blast Load using Finite Element Modelling. In: Proceedings of the 2nd International Conference on Recent Advances in Civil Engineering and Disaster Management, Peshawar, 2022, pp.1–15. https://www.researchgate.net/publication/366956656_Approximation_of_Confined_Dry-Stacked_Interlocking_Masonry_Wall_against_Blast_Load_using_Finite_Element_Modelling
26. QCVN 01:2019/BCT - National technical regulation on safety in the process of producing, testing, performing check and acceptance, storage, transportation, use, disposal of industrial explosive materials and storage of explosive precursors. Ministry of Industry and Trade, Hanoi, 2019, pp.1-162.